# Formation mechanism and control of flaring in forward tube spinning

M. Zhan [1*], J. Guo [1], M.W. Fu [2], R. Li [1], P.F. Gao [1], H. Long.[3], F. Ma [4]

[1] State Key Laboratory of Solidification Processing, School of Materials Science and Engineering, Northwestern Polytechnical University, Xi'an 710072, China

[2] Department of Mechanical Engineering, The Hong Kong Polytechnic University, Hung Hom, Kowloon, Hong Kong

3 Department of Mechanical Engineering, The University of Sheffield, Sheffield S1 3JD, UK

4 Long March Machinery Factory, China Aerospace Science and Technology Corporation, Chengdu, 610100, China

*Corresponding author: Mei Zhan, Email: zhanmei@nwpu.edu.cn;

Pls double check with Prof Zhan's name in SCI journal publication to ensure the consistency, such as M. Zhan or Mei Zhan.

Comments: The formation is discussed first and followed by evolution affected by different process parameters! Must use velocity and profile to analyse the formation of flaring!

Must discuss

1) Formation mechanism
2) How the process parameters affect the flaring formation and evolution
3) How to control and reduce the flaring

The experiment at the final stage is used to verify the validity of the simulation in such a way to prove the other simulations presented in the paper is robust and reliable,

**Abstract**

Forward tube spinning (or flow forming) is usually employed to produce cylindrically tubular components to meet the increasing requirements for manufacturing high-performance and light-weight products at low cost and short-lead time. In forward tube spinning, however, flaring defect may easily occur at the opening end of tubes, which would deteriorate the quality of the formed tubular part and reduce material utilization. Eefficient control of flaring formation is thus a non-trivial issue in forward tube spinning process and become one of the critical bottleneck issues to be addressed in forward tube spinning. In this study, the formation mechanism of flaring is systematically studied via finite element (FE) simulation and in-depth understanding is thus established, which forms basis for control of flaring forming in the process. Based on the simulated material flow behavior, it is found that flaring is formed due to that the material in non-spun zone flows away from the mandrel. This material flow behavior is caused by the pile up and the decreasing stiffness of the non-spun zone. In addition, the effects of process parameters on flaring are investigated to reduce flaring. The results show that using smaller feed rate and thickness reduction per pass can reduce maximum flaring to a certain extent, which is very limited. To increase productivity and shorten forming lead-time, an efficient method to control flaring is proposed using a pressing ring in front of the roller based on the mechanism of flaring. FE simulation is further used to study the feasibility and demonstrates the validity of the method in terms of reducing and even eliminating the flaring with a short lead-time. Finally, the forward tube spinning experiments are carried out to validate the formation mechanism of flaring and the method to

avoid or eliminate the flaring formation in forward tube spinning. .

**Keywords**: Tube spinning; Flow forming; Flaring; Forming mechanism; Flaring control and reduction .

## 1. Introduction

Tube spinning, also known as flow forming, is a forming process used to produce cylindrically tubular components [1-3]. According to the axial flow direction in tube spinning process, tube spinning is classified into two categories, namely, forward and backward spinning. In forward tube spinning process, workpiece rotates with mandrel; and one or more rollers, which revolve around their own axis, move axially along the workpiece to reduce the thickness and increase the axial length of the workpiece. Thus, the material flows in the same direction as that of the rollers, as shown in Fig. 1 [4]. While in backward tube spinning process, the material flows in the opposite direction to that of the rollers [5]. In most cases, the forward tube spinning process is usually adopted to manufacture thin-walled tubular components with a high length-diameter ratio [6]. In the forward tube spinning process, however, flaring may occur at the opening end of the workpiece (Fig. 2) [7-8]. This can easily lead to fracture at the tube end in the subsequent spinning process.

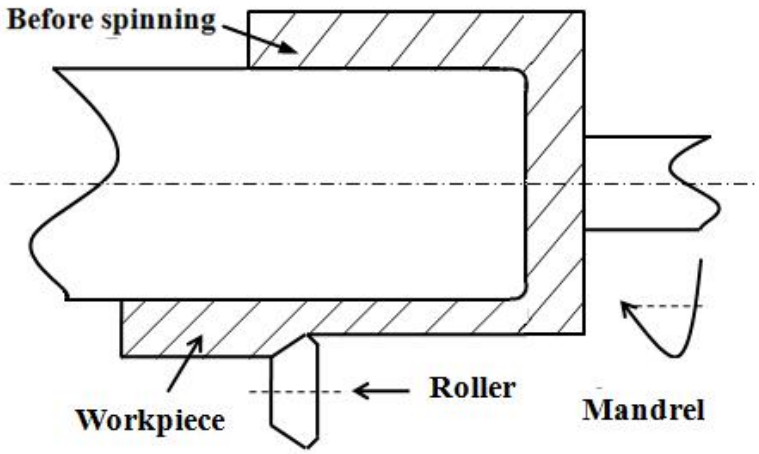


**Fig. 1** Forward tube spinning. (Good. This is an original figure. You may indicate the upper half is before spinning)

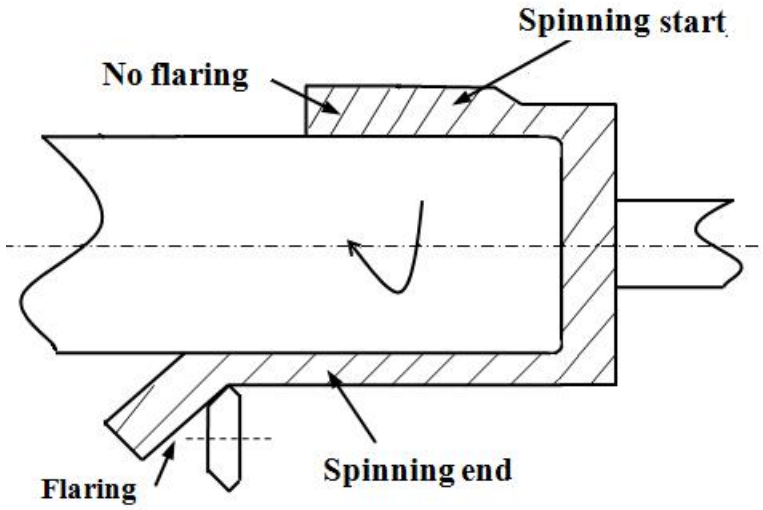


**Fig. 2** Flaring formation at the end of the tube. The representation of the symmetrical cylinder is not correct. Pls double check it

The diameter of the flared end is much larger than that of the other parts of the tubes (Fig. 2). Flaring is thus considered to be a result of the increase in diameter (or diametrical growth) of the opening end of the tube in tube spinning process [9], and much more studies have been conducted on diameter expansion than on flaring. Xu [10] noted that diameter expansion in the forward tube spinning process of steel was caused by circumferential tensile

strain. Based on the elastic-plastic finite element(FE) analysis of the forward tube spinning process, Xue et al. [11] concluded that diameter expansion and flaring were both caused by the increase of circumferential strain and stress. In addition, Song et al. [12] investigated the circumferential residual stress in forward tube spinning process through FEA and x-ray diffraction experiments. They found that tensile residual stress was much larger than shear residual stress, which contributed to the diameter expansion. Furthermore, Rajan and Narasimhan [13] revealed that the diameter expansion is a function of the ratio of the circumferential contact length to the axial contact length according to the experiments by high strength SAE 4130 steel tubes; and the smaller the ratio or the larger the thickness reduction, the greater the diameter expansion. Through flow forming experiments using the annealed AA6061 tubes, Davidson et al. [14] found that a roller feed rate in the range of 50-100 mm/min and a minimal gap between mandrel and workpiece are beneficial for avoiding diameter expansion. Fazeli and Ghoreishi [15] figured out that lower thickness reduction with thinner preform thickness, higher feed rate of rollers, slower mandrel rotational speed, and further lower solution treatment time facilitate obtaining smaller internal diameter growth and wall thickness change in the tube spinning process of 2024 aluminium alloy. Moreover, Molladavoudi and Djavanroodi [6] came out with the diameter growth increases with the increment of thickness reduction in tube spinning process.

These prior arts are mainly focused on diameter expansion occurring in the deforming zone in tube spinning process, which experiences strong constraints from rollers and the spun and non-spun zones. While flaring occurs at the opening end of the tubes in the final spinning

stage, it may experience the constraints different from those in diameter expansion [16]. This difference means that the forming mechanism and the deformation behaviours influencing flaring occurrence might not be the same as those in diameter expansion, and thus need to be systematically studied and investigated. On the other hand, how to control flaring and further to avid it in forward tube spinning process is a critical and non-trivial issue. Due to the lack of in-depth understanding of the formation mechanism of flaring and there are no effective measures to control and avoid it. The present solution is to cut off the flared end of tubes, which would reduce material utilization and increase production lead-time and cost.

In this research, the flaring formation mechanism and its evolution in tube spinning process are systematically studied by physical experiments and finite element (FE) simulation. The effects of various process parameters on flaring formation are thoroughly explored and investigated. Based on the systematic and epistemological understanding established via these explorations, an efficient method to control flaring formation is proposed. (How about the method? Whether it is efficient or not need to be clearly given there!!!!). The efficiency of developed method is validated by experiment and it provides a solution for addressing this issue in industries.

## 2. Simulation preparation and physical experiment

To reveal the instantaneous flaring formation mechanism and the material flow which lead to the formation of flaring, FE simulation is employed as it can reveal the instantaneous deformation and flow of material, which is generally impossible for physical experiment. In

addition, FE simulation has been proven to be an efficient tool for addressing metal forming design in terms of metal formed part design, process determination, tooling design and product quality control and assurance [17-19]. In tandem with this, the extensive FE simulations are conducted, together with physical experiments to study the flaring systematically in forward tube spinning process.

### 2.1 Material

The tube material used in this study is a Al-Mn1-Cu aluminium alloy and its composition is listed in Table 1. The mechanical properties was determined by tension test and the true stress- strain curve is shown in Fig. 3.

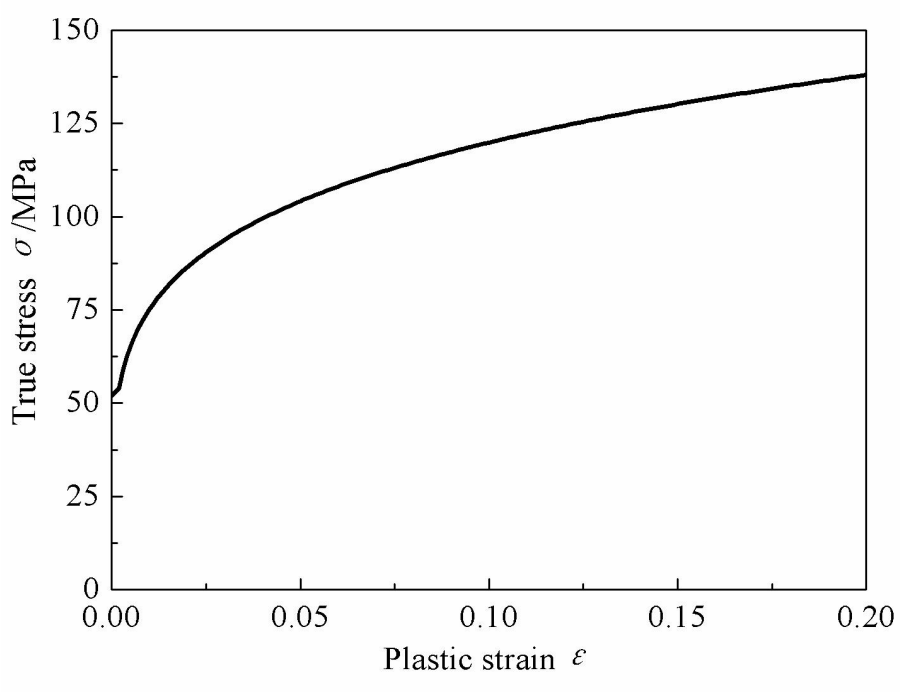


**Fig. 3** True stress- strain curve of Al-Mn1-Cu aluminium alloy.

By using the true stress-strain curve, the material constitutive model is represented by Eq. (1),

$$\sigma = \sigma_S + B\varepsilon^n \quad (1)$$

where $\sigma$ and $\varepsilon$ are the stress and strain, respectively. $\sigma_s$ is the initial yield stress and $B$ and $n$ are material constants. The material constants used in this study are shown in Table. 2

**Table 1:** Chemical composition of Al-Mn1-Cu aluminium alloy.

| Element | Al | Mn | Cu | Si | Fe | Zn |
|---|---|---|---|---|---|---|
| Content (wt%) | Matrix | 1.2 | 0.2 | 0.6 | 0.7 | 0.1 |

**Table 2:** Property parameters of Al-Mn1-Cu aluminium alloy.

| Parameters | Values |
|---|---|
| Elastic modulus $E$ (GPa) | 69.08 |
| Poisson ratio $v$ | 0.33 |
| Initial yield stress $\sigma_S$ (MPa) | 52 |
| Material constant $B$ (MPa) | 153 |
| Material constant $n$ | 0.21 |

**2.2 Simulation of forward tube spinning process**

In forward tube spinning, there exists a large plastic deformation with the nonlinearities of material, geometry and boundary. Abaqus/Explicit code was used and the three-dimensional (3D) elastic-plastic FE model is shown in Fig. 4. In the model, the tube was set as a deformable body and was meshed by an 8-node reduced integration brick element. Four layer elements were adopted along the thickness direction of the tube blank, which are sufficient to model the deformation in thickness direction in spinning process [20-22]. In addition, adaptive mesh control was applied to remesh the tube workpiece during the process. The roller and the mandrel were set as rigid body. A coupling constraint was applied to the fixed end of the tube to synchronize the tube and mandrel rotations. A velocity

boundary was applied to control the rotation of the mandrel and the axial feed motion of the roller. Coulomb's friction model was used to represent the sliding effect between tube blank, rollers and mandrel. The friction coefficients between blank, mandrel, and roller were all set as 0.1 [23]. The forming parameters are listed in Table 3.

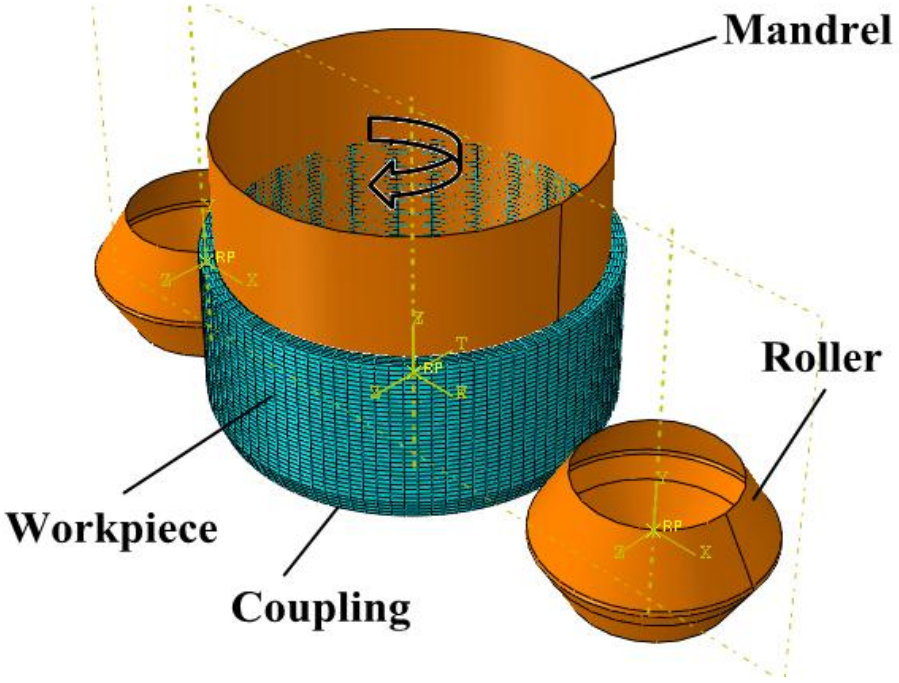


**Fig. 4** 3D elastic-plastic FE model for forward tube spinning.

**Table 3:** Forming parameters in FE simulation

| Parameters | Values | Parameters | Values |
|---|---|---|---|
| Tube blank length (mm) | 120 | Roller feed rate $f$ (mm/r) | 1.5 |
| Inner diameter of blank (mm) | 320 | Spinning pass $n_s$ | 1 |
| Blank thickness (mm) | 12 | Total thickness reduction $\psi$ (%) | 40 |
| Roller diameter (mm) | 200 | Rotation speed (r/min) | 100 |
| Roller attack angle (°) | 30 | Friction coefficient $\mu$ | 0.1 |
| Roller fillet radius (mm) | 5 | Roller feed stroke (mm) | 140 |

Theoretically, more accurate simulation results are expected by using the finer mesh, but at the cost of computation time and cost. To reasonably determine the mesh size of tube blank, the calculation accuracy and time cost of three FE models with mesh sizes of 4, 3 and 2 mm in the axial-hoop plane were compared. Table 4 shows that the maximum Mises stress, the maximum equivalent strain and computation time are all increased with the decrease of mesh size. Furthermore, the values of the maximum Mises stress were not found to change significantly under various mesh sizes. On the other hand, the difference of the maximum equivalent strain for mesh sizes of 4 and 3 mm is 12.3%, while that for mesh sizes of 3 and 2 mm is only 4.5%. These differences indicate that a mesh size less than 3 mm is good enough to simulate the tube spinning process. Considering the computational time with the mesh size of 3 mm is 39.2% less than that with the mesh size of 2 mm, the mesh size of 3 mm was thus adopted in stimulation.

**Table 4:** Simulation results under different mesh sizes.

| | Mesh size | | |
|---|---|---|---|
| | 4 mm | 3 mm | 2 mm |
| Maximum Mises stress (MPa) | 238.1 | 240.7 | 241.3 |
| Maximum equivalent strain | 4.569 | 5.210 | 5.453 |
| CPU time (h) | 99 | 248 | 408 |

In addition to the mesh size, the mass scaling factor also significantly affects the simulation results. To choose a reasonable mass scaling factor in simulation, the calculation accuracy, stability and efficiency of the model, and the internal energy, kinetic energy and computation time with four mass scaling factors were investigated, as shown in Fig. 5. In the figure, the internal energy is found to be increased with spinning time. With the decrease of

mass scaling factor, the difference of the internal energy with various mass scaling factors is increased with time and the maximum relative difference of the internal energy in different scenarios is approximately 8.1% in the final spinning stage. Fig. 5(b) shows that the kinetic energies under various scaling factors are all increased significantly in the initial spinning stage and then tended to be almost stable in the subsequent spinning stage. In addition, Fig. 5(b) also shows the increasing fluctuation of the kinetic energy in the stable stage with the increase of the mass scaling factor, which illustrates that the dynamic effect becomes increasingly significant with the increasing mass scaling. These variations of the internal and kinetic energies lead to the decrease of the ratio of kinetic energy to internal energy with spinning time, and its increase with the mass scaling factor, as shown in Fig. 5(c). Furthermore, Fig. 5(c) also shows that the initial stage in which the ratio is decreased sharply to 5% become shorter with the decrease of mass scaling factor. The curves with the mass scaling factor of 3500 and 6400 show a longer stage, in which the ratio is5% more larger than those with the mass scaling factor of 900 and 400. This indicates that a smaller mass scaling factor facilitates a more rapid transition to the stable spinning process. Fig. 5(d) shows that with the increase of mass scaling factor, computation time decreases remarkably. For a reliable FE simulation of the spinning process, the maximum ratio of kinetic energy to internal energy must be less than 10%, and the kinetic energy curve must be free of any sudden fluctuation [24-28]. Based on the this discussion, it can be concluded that the energy variation under the mass scaling factor of 900 and 400 are within the limit for a reliable FE simulation of the spinning process. This indicates that dynamic effect in the spinning process

is not significant and can be negligible in these two mass scaling factors. Furthermore, considering that the computation time with the mass scaling factor of 400 is approximately 1.5 times longer than that with the mass scaling factor of 900, the rational mass scaling factor for simulation was confirmed as 900.

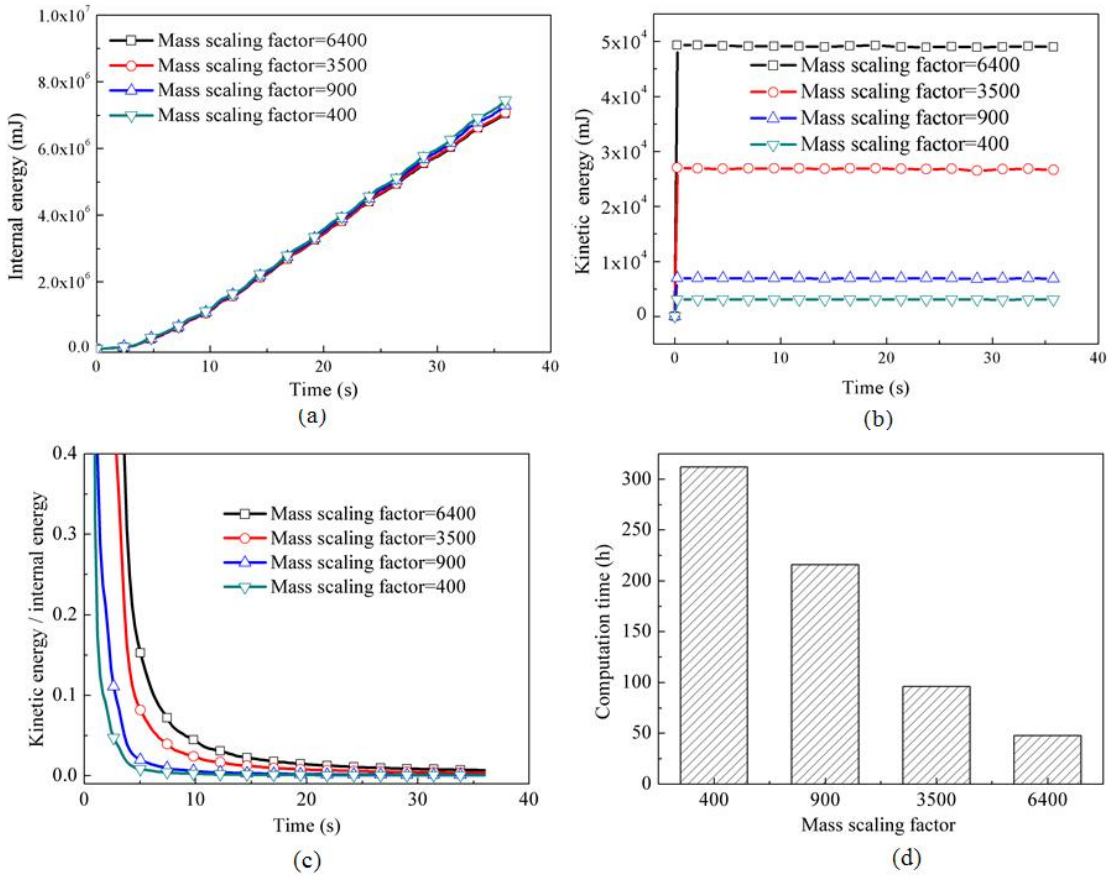


**Fig. 5** Variations of (a) internal energy, (b) kinetic energy, (c) ratio of kinetic energy to internal energy, and (d) computation times under different mass scaling factors.

## 2.3 Forward tube spinning experiment

The forward tube spinning experiments were conducted on a CZ900/2CNC spinning

machine, as shown in Fig. 6. The blank used in the experiments were cut from tubes. To make the tube blank rotate synchronously with the mandrel, a fixed end was manufactured at the bottom end of the blank and a designed fixed die was inserted into the fixed end, as shown in Fig. 7. During the experiments, the tailstock was forced to press the fixed die to make the tube blank rotate synchronously with the mandrel. The forming parameters are the same as those in Table 3. The blank surface was coated with $MoS_2$ on as lubricant. Furthermore, coolant was also used through the experiments process to avoid rapid temperature rise of spun tube.  This section is quite short!!

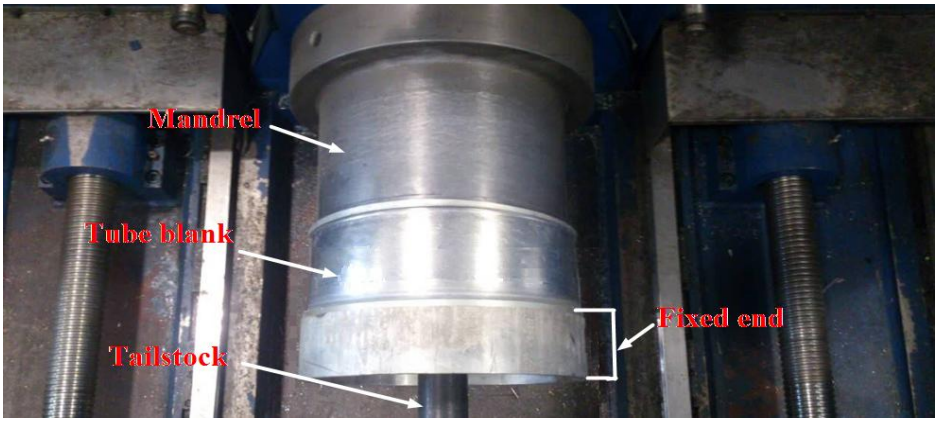


**Fig. 6** Tube blank on mandrel.

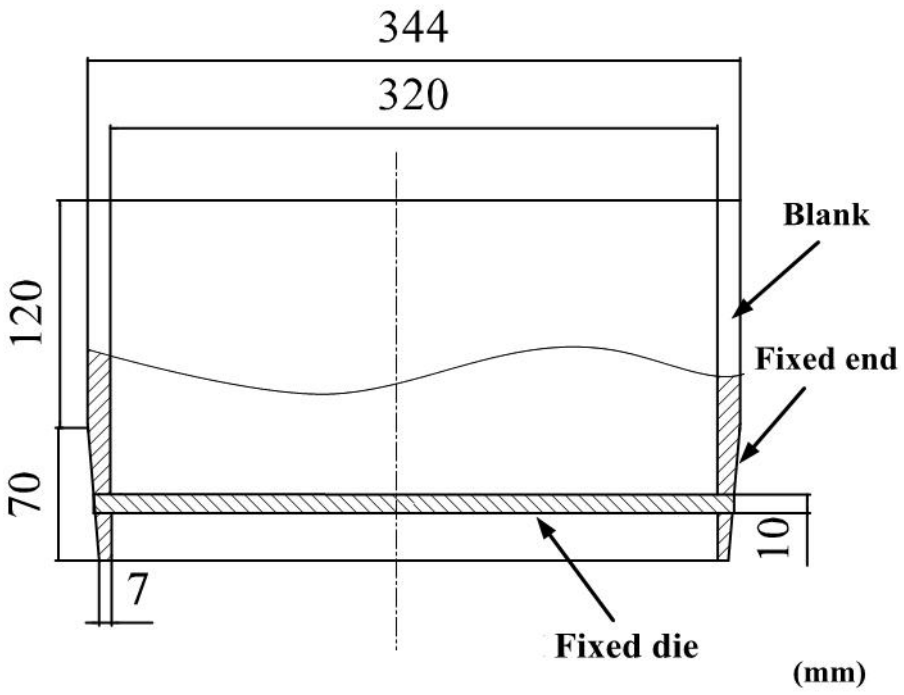


**Fig. 7** Sketch of fixed end of blank and fix die.

## 3. Flaring formation and influencing parameters

In this section, the formation of flaring in forward tube spinning process and the effects of process parameters on flaring are studied.

### 3.1 Formation mechanism

Based on the FE simulation of forwards tube spinning process, the formation of flaring can be divided into two main stages, as shown in Fig. 8. Firstly, when the roller moves forward, the material in front of the roller accumulates and pile up is formed. Due to the formation of pile up, the material in front of the roller further flows upwards and backwards and moves away from the mandrel. Bulge up is then formed between the flowing material and mandrel. At the same time, the material in the non-spun zone still flows forwards and

show no tendency to move away from the mandrel. Then, the roller keeps moving forwards, the materials in the non-spun zone moves away from the mandrel and a gap is formed between the material and mandrel, stage 2 begins. In stage 2, due to the formation of pile up, the material still flows upwards and the material in front of the roller keeps moving away from the mandrel. Meanwhile, due to the formation of bulge up and the decreasing length of the non-spun zone, the stiffness of the non-spun zone significantly reduces. When the stiffness of the non-spun zone decreases to a certain value, the material in the non-spun zone is being affected by the pile-up. It flows upwards and forwards, and moves away from the mandrel. This flow pattern finally develops a flaring and the maximum flaring would appear when pile up disappears, as shown in Fig. 8.

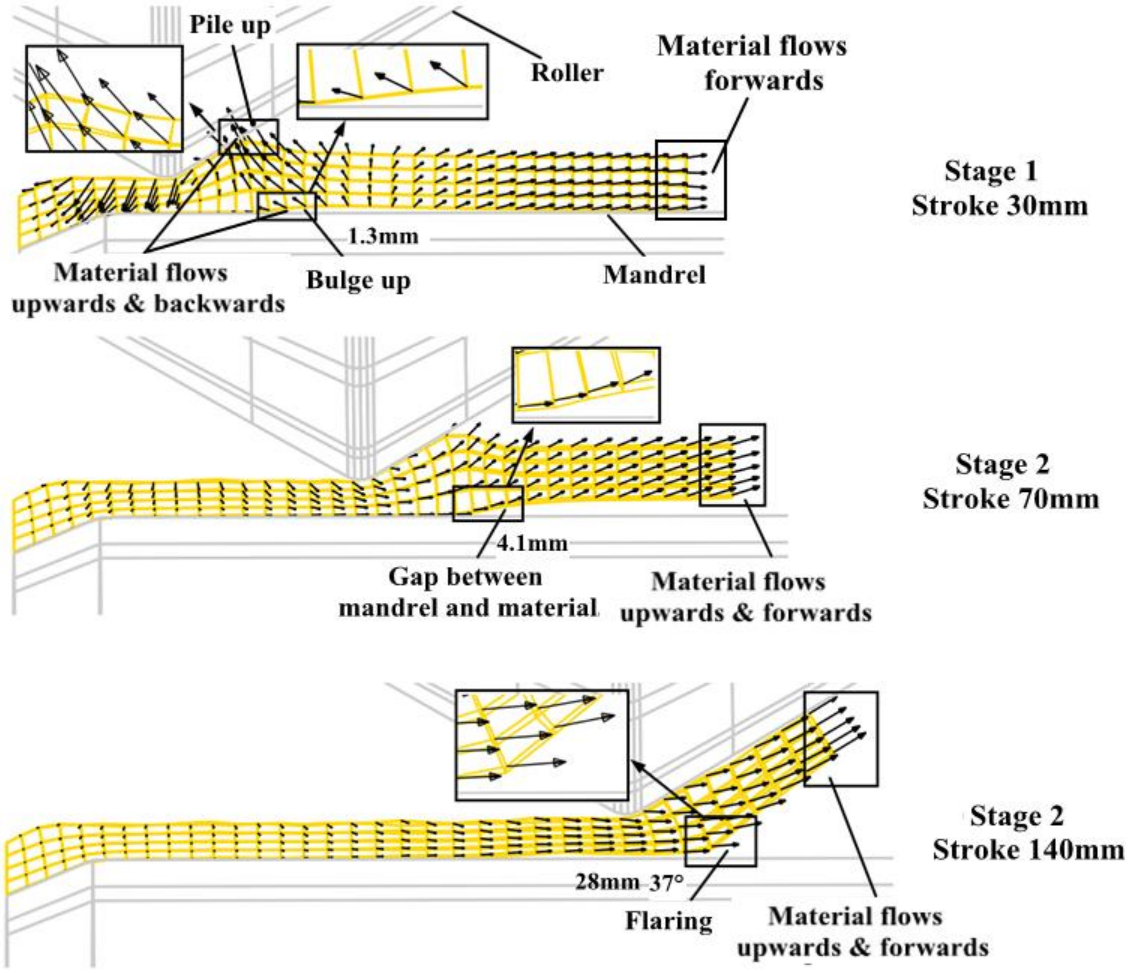

**Fig. 8** Formation mechanism of flaring in forward tube spinning process.

### 3.3 Flaring influencing parameters

Based on the revealed flaring formation mechanism, it is firstly suggested in this research to introduce optimized parameters to make the material just flow forwards along the mandrel for the purpose to avoid the formation of flaring. Therefore, based on the FE model established in Section 2.2, a group of simulations was designed using the single factor analysis method, as shown in Table 5, to study the effects of process parameters (roller feed rate, roller fillet radius, roller attack angle, thickness reduction and thickness distribution in multiple passes) on the evolution and formation of flaring and also to control flaring in the process. The flaring is evaluated by the flaring angle and the axial length of flaring. The larger flaring angle and axial length indicates that the flaring is more severe.

**Table 5:** Research plan for single factor analysis.

| Parameters / No. | Roller feed rate $f$ (mm/r) | Roller attack angle $\alpha$ (°) | Roller fillet radius $R_r$ (mm) | Spinning pass $n_s$ | Reduction per pass $\psi_i$ (%) | Total reduction $\psi$ (%) |
|---|---|---|---|---|---|---|
| 1 | 0.5 | 30 | 5 | 1 | 40 | 40 |
| 2 | 1 | 30 | 5 | 1 | 40 | 40 |
| 3 | 1.5 | 20 | 5 | 1 | 40 | 40 |
| 4 | 1.5 | 25 | 5 | 1 | 40 | 40 |
| 5 | 1.5 | 30 | 1.5 | 1 | 40 | 40 |
| 6 | 1.5 | 30 | 3 | 1 | 40 | 40 |
| 7 | 1.5 | 30 | 5 | 1 | 20 | 20 |
| 8 | 1.5 | 30 | 5 | 1 | 60 | 60 |
| 19 | 1.5 | 30 | 5 | 3 | 20 | 60 |

#### 3.3.1 Effect of roller feed rate

Fig. 9 shows the simulation results of the material flow behavior with different feed rate.

When the feed rate is 0.5mm/r, the material under the roller does not have the tendency to move away from the mandrel before the feed stroke of 70mm though pile up is formed. Thus, no bulge up and gap is formed. The flaring is formed directly when the non-spun zone decreases to a certain length, in which the stiffness of non-spun zone is reduced and the non-spun zone is being affected by the pile-up and the material flows upwards. As the non-spun zone has better stiffness without bulge up and gap. The flaring is formed with shorter non-spun length compared with those under larger feed rate. The flaring angle at the feed stroke of 140mm is much smaller than that under the feed rate of 1 mm/r and 1.5 mm/r. While when the feed rate is 1mm/r, the flaring formation is similar with that under the feed rate of 1.5mm/r with smaller bulge up, gap and flaring at the same feed stroke (Fig. 8). This is due to that under a smaller feed rate, the material smoothly flows along the axial direction, resulting in smaller pile up. With the smaller pile up, the trend of material flows upwards also decreases. Furthermore, it needs to be noted that the flaring would keep growing when the feed stroke exceeds 140mm under the smaller feed rate of 0.5mm/r and 1mm/r, as shown in Fig. 9. The maximum flaring were found to appear with larger feed stroke under smaller feed rate. The maximum flaring angle and axial length are all found to decrease with the decrease of feed rate, which indicates that smaller feed rate is helpful to control flaring formation.

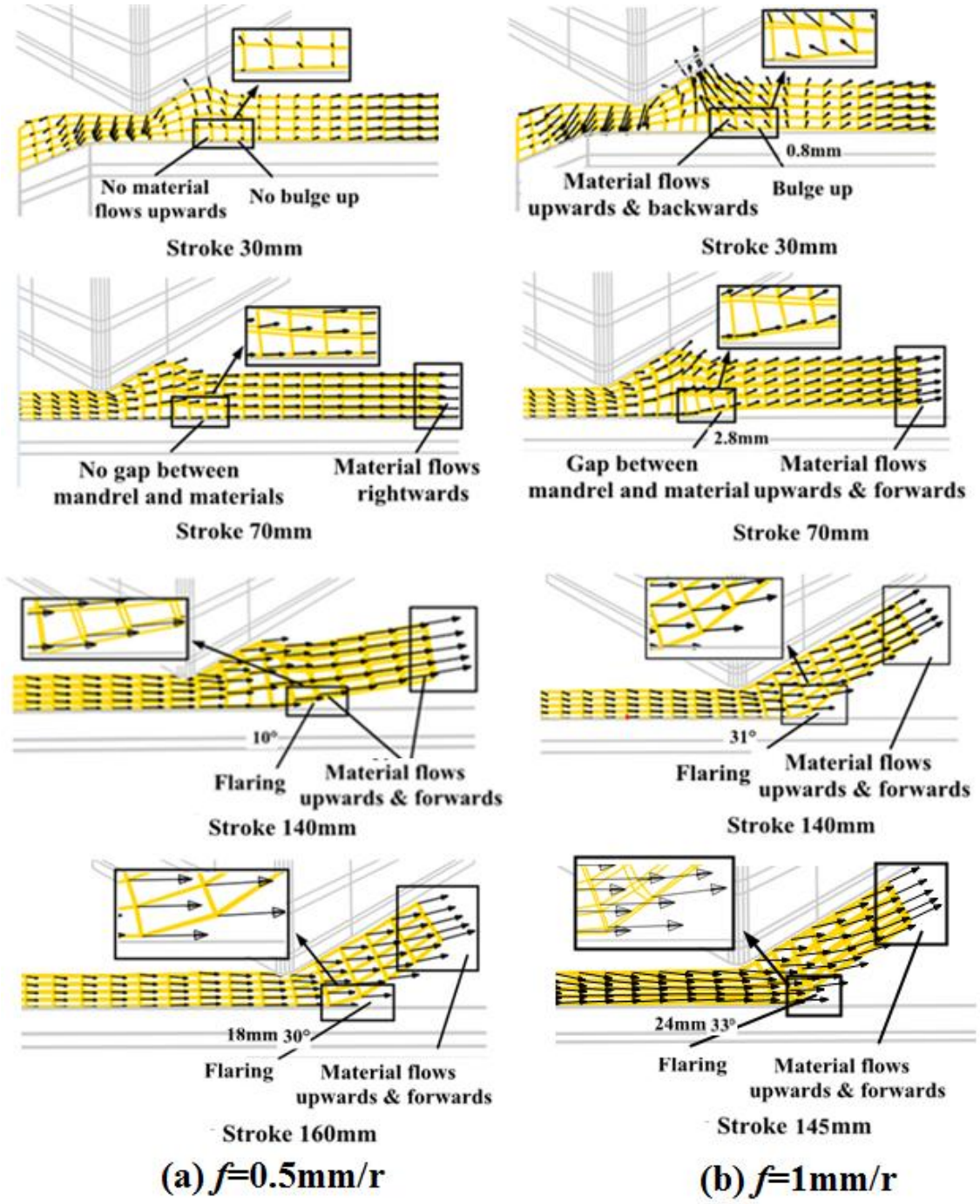


**Fig. 9** Flow behaviors with different feed rates: (a) $f$=0.5mm/r, (b) $f$=1mm/r.

### 3.3.2 Effect of roller attack angle

Fig. 10 shows the simulation results of the material flow behavior with different attack angles. It can be found that the flaring formation is similar under different attack angles. The

bulge up and pile up decrease with the increase of attack angle. This is due to that with smaller attack angles, the contact length between the roller and blank increases, leading to the decrease of the axial material flow and the increase of circumferential material flow, which in turn causes larger bulge up and gap. However, under smaller attack angle, the larger bulge up and gap would not lead to larger flaring angle. As the flaring development is constrained by the rollers. When the flaring grows to the attack angle, it will stop increasing. Thus, the maximum flaring angle under larger attack angle is larger than those under smaller attack angles. However, the maximum flaring axial length under larger attack angle is found to be smaller than those under smaller attack angles. Those results indicate that smaller or larger attack angle would both lead to more severe flaring.

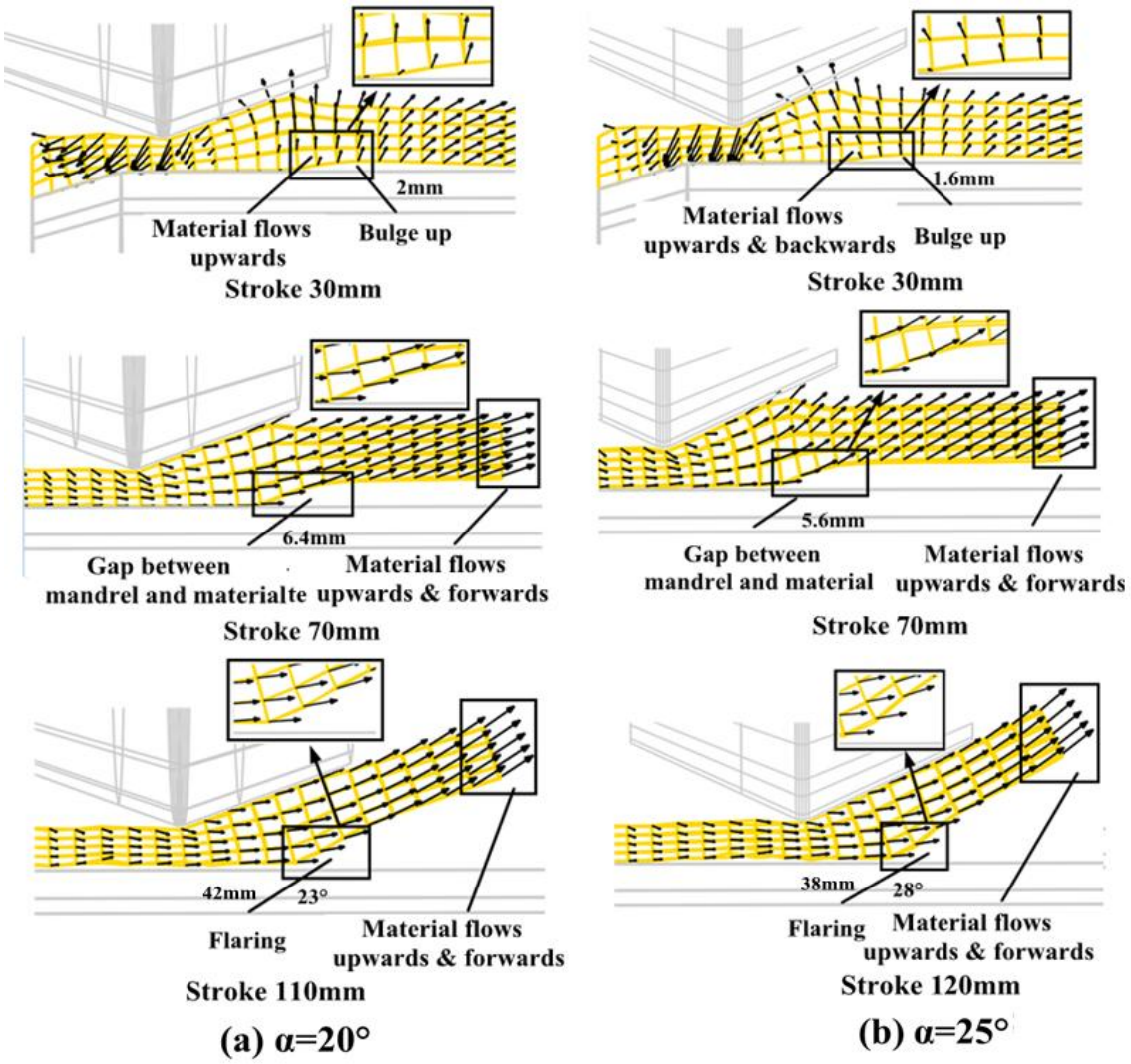


**Fig. 10** Flow behaviors with different attack angles: (a) $\alpha$=20°, (b) $\alpha$=25°.

### 3.3.3 Effect of roller fillet radius

Fig. 11 shows the simulation results of the material flow behavior with different roller fillet radius. It can be also found that the flaring formation is similar under different roller fillet radius. The maximum flaring all appears at the feed stroke of 140mm. It is found that the maximum flaring angle and axial length all increase slightly with the increase of roller fillet radius. This is because the increase of the roller fillet radius increases the contact area

between the roller and the workpiece. An increased amount of material under the contact area implies that more material must flow in the axial direction, resulting in greater material accumulation in front of the roller. This leads to a slight increase in the pile-up in front of the roller and thus an increased bulge up, gap and flaring angle.

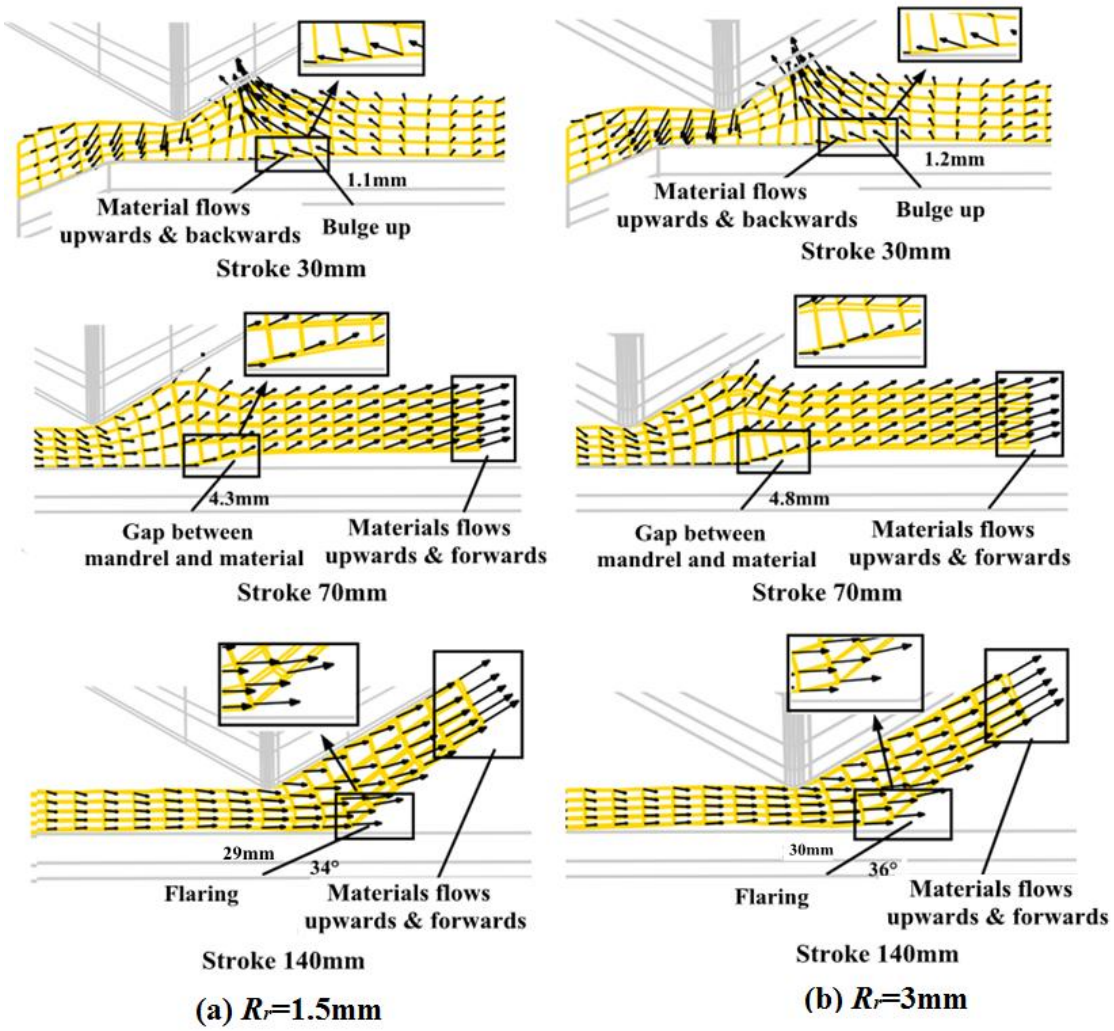


**Fig. 11** Flow behaviors with different roller fillet radius: (a) $R_r$=1.5mm, (b) $R_r$=3mm.

### 3.3.4 Effect of thickness reduction

This section firstly investigates the effects of various thickness reductions in a single pass on flaring. Then, effects of total thickness reduction and the distribution of a given total

thickness reduction in multiple passes were studied.

#### 3.3.4.1 Effect of thickness reduction in single pass

Fig. 12 shows the simulation results of the material flow behavior with different thickness reduction. When the thickness reduction is 20%, the bulge up and gap is not formed before the feed stroke of 70mm. This is due to that under a small thickness reduction results in small pile up. The small pile up would not make the material near the mandrel flow upwards. The flaring is formed in the final stage in which the stiffness of the non-spun zone decreases to a certain value, and being affected by the pile up. At the feed stroke of 140mm, the flaring is found to be smaller than those under the thickness reductions of 40% and 60%. Furthermore, the maximum flaring and axial length is also found to be smaller than those under the thickness reductions of 40% and 60% e. While when the thickness reduction is 60%, the flaring formation is similar as that under the thickness reduction thickness 40%. Compared with smaller thickness reduction, larger pile up is formed under this condition, thus leading to a larger bulge and gap, and finally results in larger flaring angle and axial length. This indicates that smaller reduction in single pass is helpful to control flaring formation.

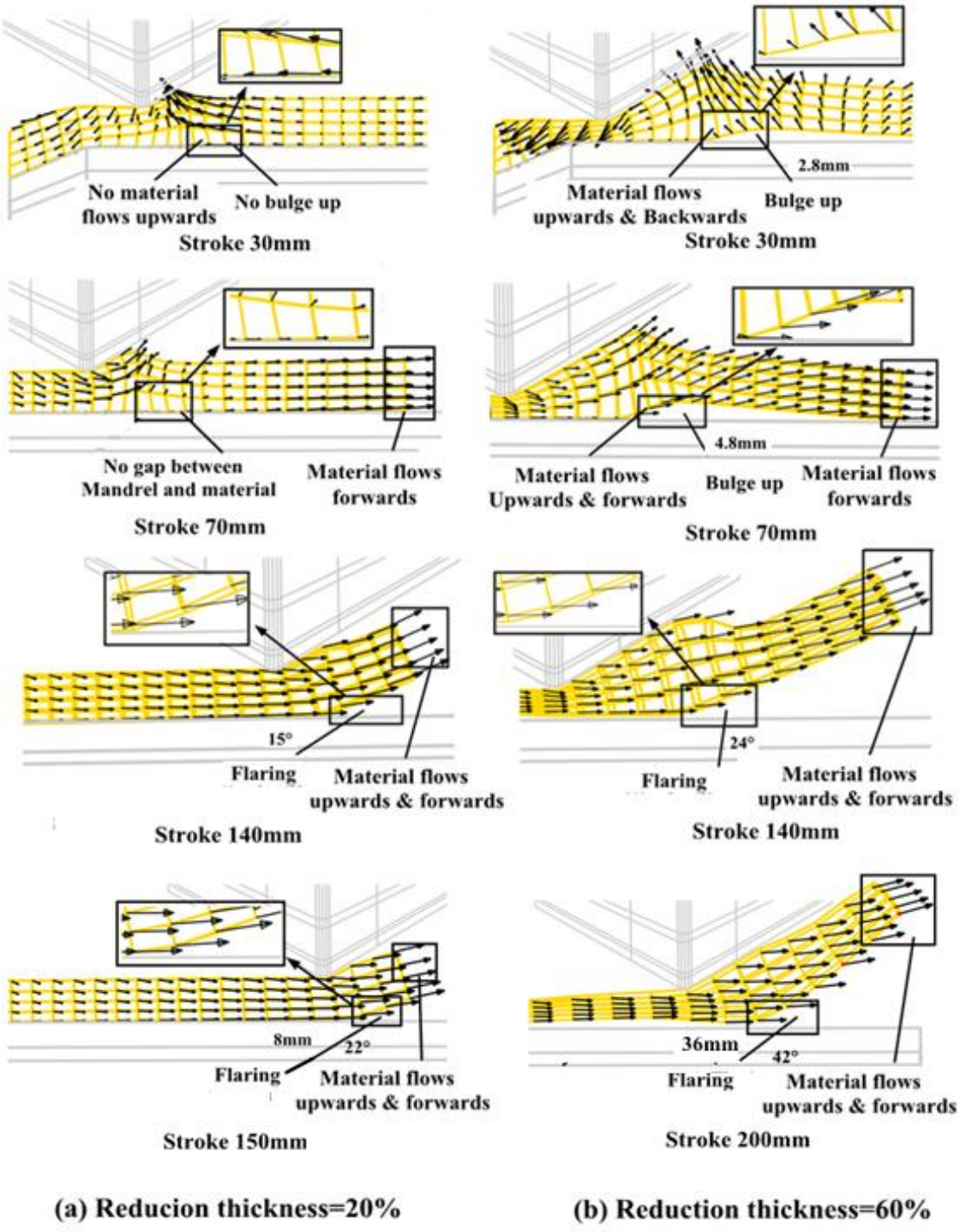


**Fig. 12** Flow behaviors with thickness reduction: (a) reduction thickness=20%, (b) reduction thickness=60%.

### 3.3.4.2 Effect of thickness reduction in multiple pass

Fig.13 shows the simulation results of the material flow behaviors in second and third

passes under a total reduction of 60% with the same thickness reduction per pass (thickness reduction 20%). In the second pass, it can be found that very small bulge up is formed and then gradually grows up. In the final stage of the second pass. The flaring is formed due to the decreasing length of non-spun zone. Compared with the spinning process with one single pass with the thickness reduction of 40% (Fig. 8), it can be found that the maximum flaring angle and axial length with two passes is smaller and appears with larger feed stroke. While in the third pass, it can be clearly found that large bulge up appears and gradually grows up, resulting in large flaring angle and axial length. Compared with the spinning process with one single pass with thickness reduction of 60% (Fig. 12), three passes spinning would not help to decrease the flaring. For the thickness reduction of 60%, more spinning passes with smaller thickness reduction per pass are needed for flaring control.

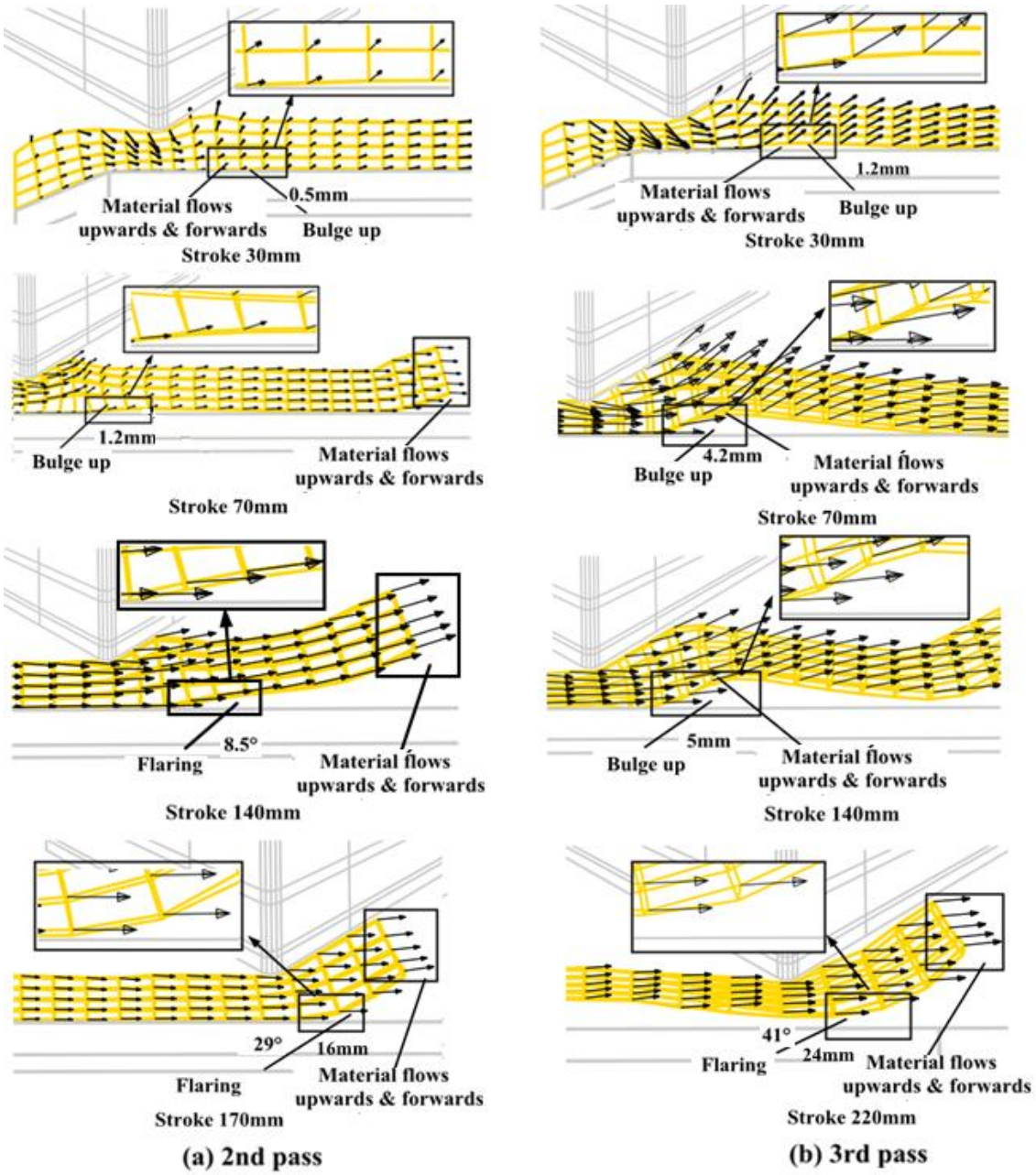


**Fig. 13** Flow behaviors with different spinning passes: (a) 2nd pass, (b) 3rd pass.

## 4. Control and reduction of flaring

Based on the investigation of the influence of process parameters in Section 3.3, it can be concluded that under decreasing thickness reduction per pass and the roller feed rate can help to decrease flaring to a certain extent. However, these decrease is very limited.

Furthermore, the spinning process under these parameters has a long forming-lead time. This makes it difficult to attain high-performance and light-weight tubes through spinning with productivity.

For these reasons, a control method to efficiently reduce and even eliminate flaring in the forward tube spinning process is needed. Based on the analysis of the forming mechanism in Section 3, it is known that flaring is mainly cause by pile-up. Therefore, a method to control flaring in the forward tube spinning process is proposed here, by installing a pressing ring in front of the roller, as shown in Fig. 14. As the pressing ring is fixed on the axle of the roller, it can move axially with the roller and rotate during the spinning process. Therefore, the pressing ring can suppress the pile-up in front of the roller and thus the flow away tendency of materials from the mandrel.

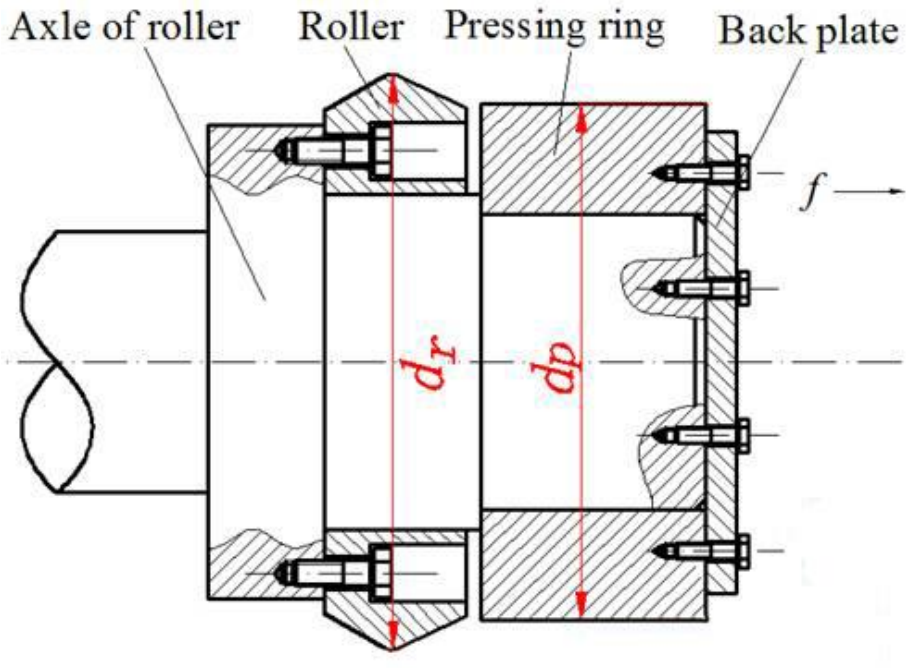


**Fig. 14.** Pressing ring fixed on the axle of the roller.

Considering the relative positions of the pressing ring and the roller, the thickness

reduction, and the need to constrain the pile-up in front of the roller, the outside diameter of the pressing ring should be slightly smaller than the difference in the diameter of the roller and the thickness reduction. Therefore, the outside diameter of the pressing ring can be determined by Eq. (2) ,

$$d_p = d_r - 2\psi - mt_0 \tag{2}$$

where $d_p$ is the outside diameter of the pressing ring, $d_r$ stands for the roller diameter, $\psi$ is the total thickness reduction, $t_0$ is the initial wall thickness of the tube blank, $m$ is a coefficient in the range of 0.2- 0.4 to define the initial gap between the press ring and blanks under different thickness reductions. The initial gap could prevent the friction caused by the unnecessary contact between the press ring and the blank in the initial stage of spinning process. The length of the pressing ring can be set as approximately 3-5 times the thickness of the tube blank, since the length of the non-spun zone approximately reaches the value when flaring occurs.

In this method, the pressing ring can constrain the formation of the pile-up in front of the roller and the outward rotation effect of the non-spun zone, finally controlling the flaring at the end of tube spinning. This method is similar to that of the special roller with a specific shape fillet, suggested by Klocke and Knig [29], as shown in Fig. 15. The separate structural design of the pressing ring with the roller makes enables flexible matching of pressing rings to rollers with different radii. This makes the pressing ring suitable for different spinning processes with different thickness reductions, in contrast to the design of the fillet size of the special roller suggested by Klocke and Knig. This difference in these two structures indicates

that the method in this study is more flexible.

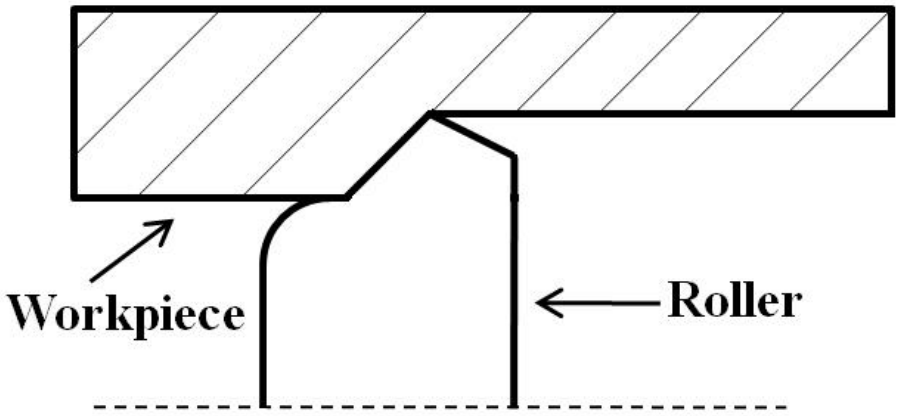


**Fig. 15.** Special roller suggested by Klocke and Knig [29].

To verify the feasibility of the proposed method for controlling flaring, a 3D FE model of forward tube spinning with a pressing ring (Fig. 16) was established, based on the 3D FE model without the pressing ring in Section 2.2. In the model with the pressing ring, all the process parameters are the same as those in Section 2.2 and Table 3. The pressing ring was set to have a length of 45 mm and a diameter of 186.8 mm by using a coefficient of 0.3 for *m*.

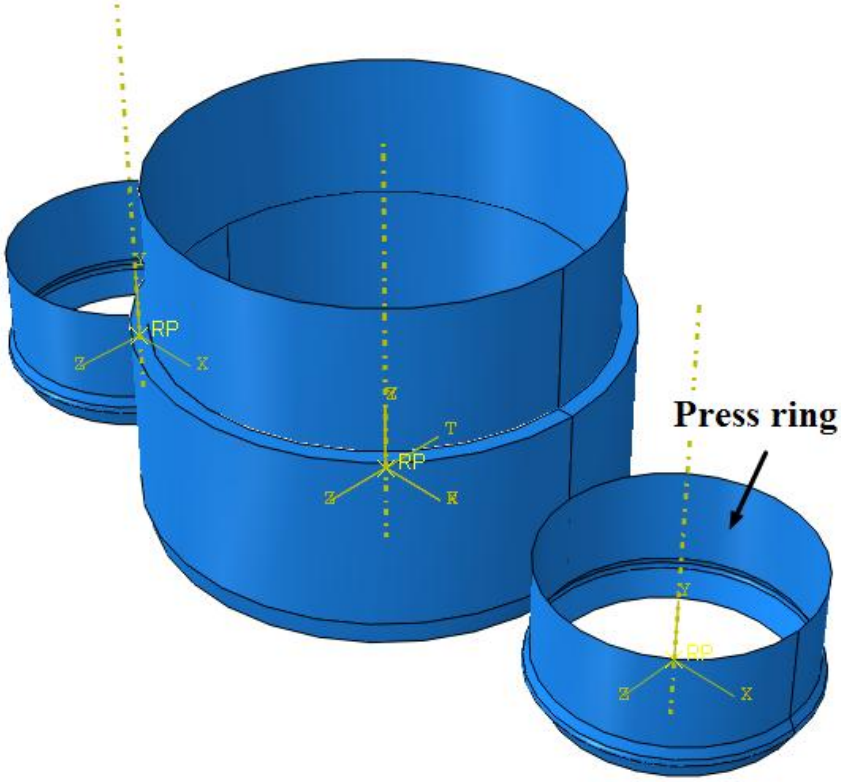


**Fig. 16.** 3D FE model for forward tube spinning with a pressing ring.

The material flow behavior with flaring was shown in Fig. 17. With the feed stroke of 30mm, it can be found that no pile up is formed under the action of press ring. Thus, the material under the roller flows forwards and shows no tendency of flowing upwards, resulting no bulge up. As roller moves forwards, at the feed stroke of 70mm, the material under the roller still moves forwards, while the material in the non-spun zone also flow forwards. Thus, no gap is formed between the mandrel and material. When the roller moves to the end of the workpiece with a feed stroke of 210mm, it can be clearly found that no flaring is formed, which indicated that the pressing ring could prevent the formation of flaring efficiently.

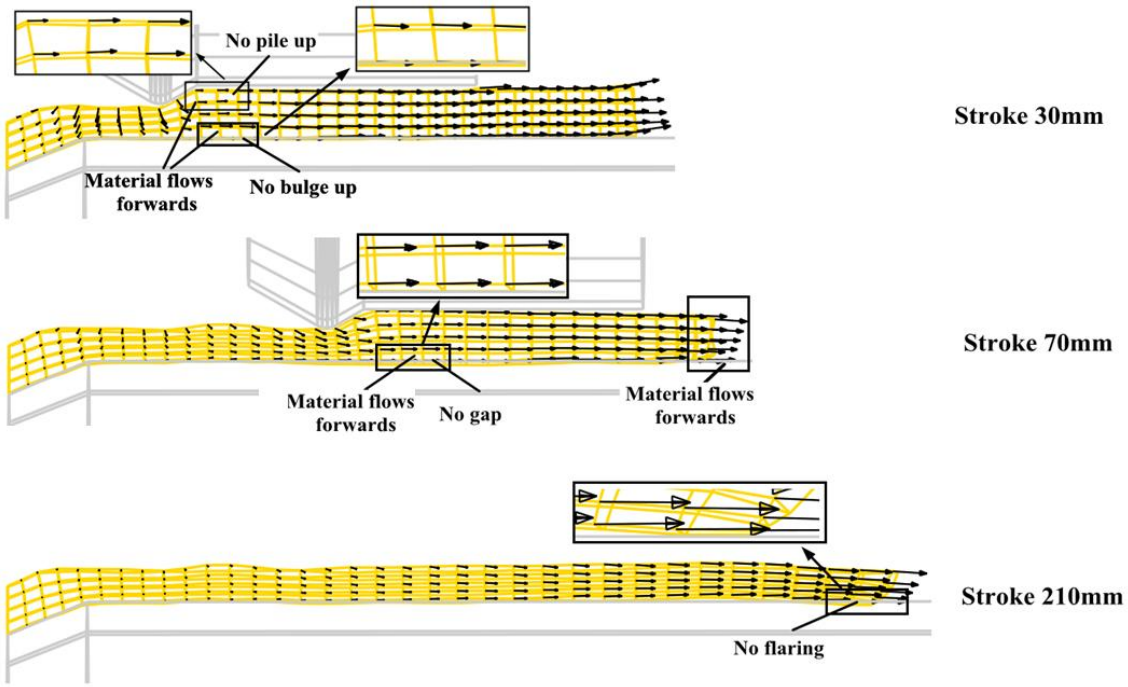


**Fig. 17.**Material flow behaviors with pressing ring.

## 5. Experiment study

The forward tube spinning experiments at the roller feed rate of 0.5, 1.0 and 1.5 mm/r are identified as cases study in this research. The longitude section of spun tube at the feed stroke of 140mm are shown in Fig. 18. It can be found that flaring also occurs in the experiments, and the flaring increases with the increase of feed rate. The flaring angles got in experiments are found to show no large difference with those got in simulations, as shown in Fig.19.

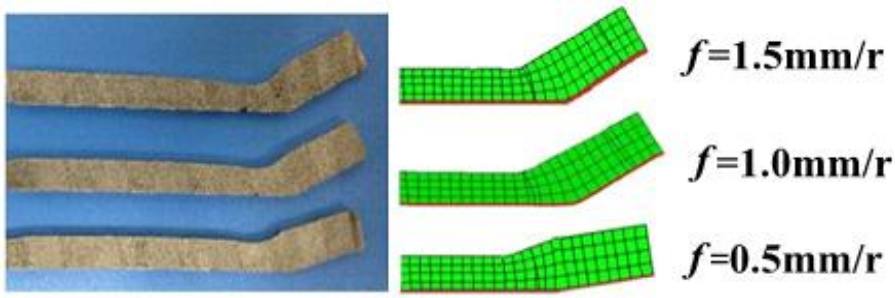

**Fig. 18** Flaring got in experiments and simulations at the same feed stroke.

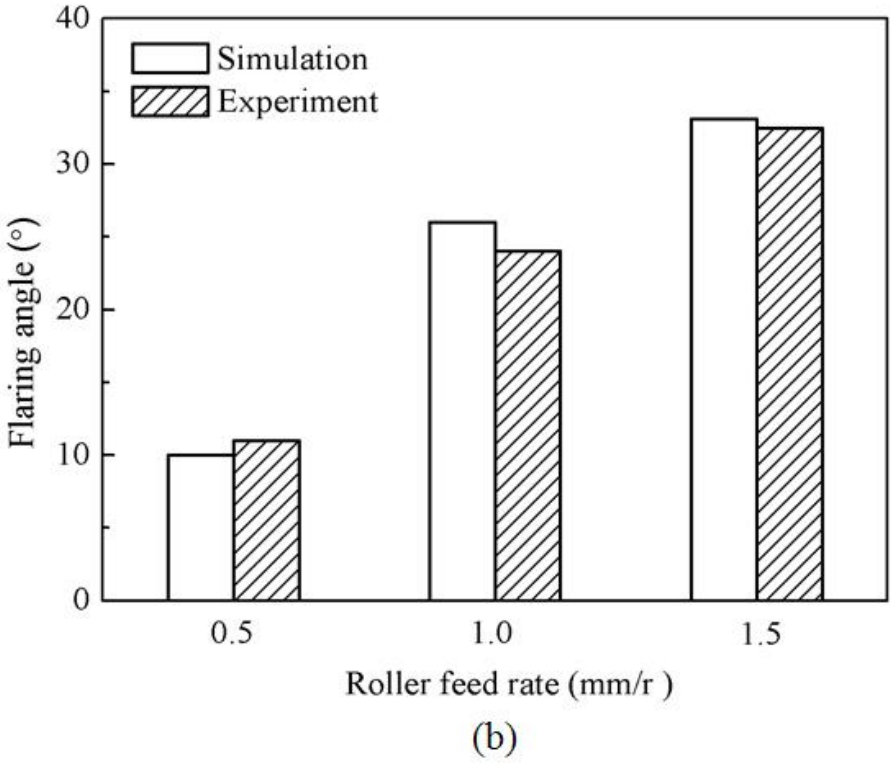


**Fig. 19** Comparisons of flaring between experiments and simulations.

To avoid flaring, a pressing ring is designed based on the simulation in Section 4, as shown in Fig. 20. Fig. 21 shows the spun tube with pressing ring. It can be found that no flaring appears in the spun tube, which indicates that the pressing ring design is an effective method to reduce and even eliminate flaring. It is worth noting that the spinning experiment was accomplished under a large roller feed rate of 1.5 mm/r, and a large thickness reduction in a single pass (60%). This further indicates that this is a efficient method to reduce and even eliminate flaring under a large roller feed rate and thickness reduction per pass with productivity.

**Fig. 20.** The pressing ring used in experiments.

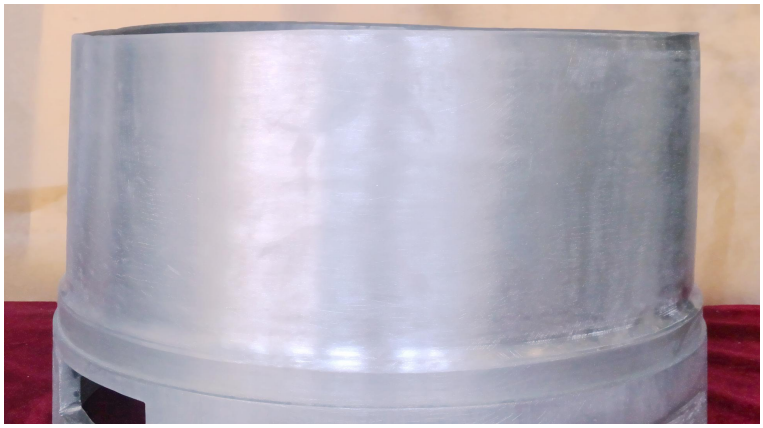

**Fig. 21.** Spun tubes with pressing ring..

**. Conclusions**

The formation mechanism, influencing parameters and control method of flaring were investigated through FE simulation on the forward tube spinning of a Al-Mn1-Cu aluminium alloy. The main conclusions are as follows:

(1) In the forward tube spinning process, the formation of flaring is formed as the material in the non-spun zone flows away from the mandrel. This material flow behavior is caused by the pile up and decreasing non-spun zone stiffness.

(2) Smaller roller feed rate and thickness reduction per pass are the key factors influencing flaring formation. For a spinning process with a large total thickness reduction, it is useful

to use multiple passes, and small thickness reduction per pass, roller feed rate, to decrease flaring to a certain extent. However, the flaring decrease is very limited and such a spinning process has a long forming lead-time.

(3) A method involving the installation of a pressing ring in front of the roller is proposed to control flaring by suppressing the pile-up. The FE simulations and experiments show that it is an effective and efficient method for reducing and eliminating flaring with short forming time.

## Acknowledgements

The authors acknowledge support from the National Science Fund for Excellent Young Scholars of China (Project 51222509), Key Program Project of the Joint Fund of Astronomy and National Natural Science Foundation of China (Project U1537203) and Research Fund of the State Key Laboratory of Solidification Processing (Projects 97-QZ-2014 and 90-QP-2013). The authors also acknowledge the partial support of the EU FP7 Marie Curie International Research Staff Exchange Scheme (IRSES, MatProFuture, project no: 318968).

## References

[1] Wong CC, Dean TA, Lin JG (2003) A review of spinning, shear forming and flow forming processes. Int J Mach Tools Manuf 43(14): 1419–1435

[2] Music O, Allwood JM, Kawai K (2010) A review of the mechanics of metal spinning. J Mater Process Technol 210(1): 3-23

[3] Parsa MH, Pazooki AMA, Ahmadabadi MN (2009) Flow-forming and flow formability simulation.

Inter J Adv Manuf Tech 42(5-6): 463-473

[4] Xu WC, Zhao XK, Ma H, Shan DB, Lin H (2016) Influence of roller distribution modes on spinning force during tube spinning. Inter J of Mech Sci 113: 10-25

[5] Zhao GY, Lu CJ, Zhang RY, Guo ZH, Zhang MY (2017) Uneven plastic deformation behavior of high-strength cast aluminum alloy tube in multi-pass hot power backward spinning. Inter J Adv Manuf Tech 88(1): 907-921

[6] Molladavoudi HR, Djavanroodi F (2011) Experimental study of thickness reduction effects on mechanical properties and spinning accuracy of aluminum 7075-O, during flow forming. Inter J Adv Manuf Tech 52(9): 949-957

[7] Luo B, Li X, Zhang X, Luo Y (2015) Drum instability of thinning spinning ultra thin-walled tubes with large diameter-to-thickness ratio. J Cent South Univ 22(7): 2456-2462

[8] Zhao XK, Xu WC, Chen Y, Ma H, Shan DB, Lin H (2017) Fabrication of curved generatrix workpiece of TA15 titanium alloy by variable thickness tube spinning and flaring process. Inter J Adv Manuf Tech 88(5):1983-1992

[9]Mohebbi MS, Akbarzadeh A (2010) Experimental study and FEM analysis of redundant strains in flow forming tubes. J Mater Process Technol 210(2): 389-395

[10] Xu D (1989) Thickness reduction spinning of the thin-walled cylinder with inner stiffness. In: Proceedings of the Fourth International Conference of Rotary Forming: 17-21

[11] Xue KM, Wang Z, Lu Y, Li KZ (1997) Elasto-plastic FEM analysis and experimental study of diametral growth in tube spinning. J Mater Process Technol 69 (1-3): 172–175

[12] Song X, Fong KS, Oon SR, Tiong WR., Li PF (2014) Diametrical growth in the forward flow forming

process: simulation, validation, and prediction. Inter J Adv Manuf Tech 71 (1- 4): 207-217

[13] Rajan KM, Narasimhan K (2001) An investigation of the development of defects during flow forming of high strength thin wall steel tubes. ASM J Pract Failure Anal 1(5): 69-76

[14] Davidson MJ, Balasubramanian K, Tagore GRN (2008) An experiment study on the quality of flow-formed AA6061 tubes. J Mater Process Technol 203(1): 321-325

[15] Fazeli AR, Ghoreishi M (2011). Statistical analysis of dimensional changes in thermomechanical tube-spinning process. Inter J Adv Manuf Tech 52(5-8): 597-607

[16] Rasoli MA, Abdullah A, Farzin M, Fadaei TA (2012) Influence of ultrasonic vibrations on tube spinning process. J Mater Process Technol 212(6): 1443-1452

[17] Fu MW (2016) Design and Development of Metal Forming Processes and Products aided by Finite Element Simulation, Springer-Verlag London Ltd..

[18] Fu MW, Yong MS and Muramatsu T (2008) Die fatigue life design and assessment via CAE simulation. Int J of Adv Manuf Techno., 35, 843-851.

[19] Fu MW, Yong MS, Tong KK, Muramatsu T (2008) Design solution evaluation for forming product development via CAE simulation, Int J of Adv Manuf Techno., 38, 249-257.

[20] Zhang JH, Zhan M, Yang H, Jiang ZQ, Han D (2012) 3D-FE modeling for power spinning of large ellipsoidal heads with variable thicknesses. Comput Mater Sci 53(1): 303-313

[21] Zhan, M, Zhang T, Yang H, Li LJ (2016) Establishment of a thermal damage model for Ti-6Al-2Zr-1Mo-1V titanium alloy and its application in the tube rolling-spinning process. Inter J Adv Manuf Tech 87(5-8): 1345-1357

[22] Yang H, Li H, Zhan M (2010) Friction role in bending behaviors of thin-walled tube in

rotary-draw-bending under small bending radii. J Mater Process Technol 210(15): 2273–2284

[23] Ma F, Yang H, Zhan M (2010) Plastic deformation behaviors and their application in power spinning process of conical parts with transverse inner rib. J Mater Process Technol 210(1): 180-189

[24] Abaqus Analysis User's Manual (2003) ABAQUS Inc. Version 6.4

[25] Bai Q, Yang H, Zhan M (2008) Finite element modeling of power spinning of thin-walled shell with hoop inner rib. Trans Nonferrous Met Soc China 18: 6-13

[26] Essa K, Hartley P (2009) Numerical simulation of single and dual pass conventional spinning processes. Int J Mater Form 2: 271–281

[27] Huang L, Yang H., Zhan M, Hu LJ (2008) Numerical simulation of influence of material parameters on splitting spinning of aluminum alloy. Trans Nonferrous Me. Soc China 18: 674-681

[28] Wang L, Long H (2011) Investigation of material deformation in multi-pass conventional metal spinning. Mater Des32(5): 2891–2899

[29] Klocke F, Knig W (2006) Fertigungsverfahren Umformen, 5th edition (German). pp 390-393